Surface Structures in the SMSI State; Pd on (1 × 2) Reconstructed TiO_2(110)

R. A. Bennett,[†,‡] C. L. Pang,[†] N. Perkins,[†] R. D. Smith,[†] P. Morrall,[†] R. I. Kvon,[†,§] and M. Bowker*[,†]

Centre for Surface Science and Catalysis, Department of Chemistry, The University of Reading, Reading, RG6 6AD, U.K., Department of Physics, The University of Reading, Reading, RG6 6AF, U.K., and Boreskov Institute of Catalysis, Novosibirsk 630090, Russia

Received: October 16, 2001; In Final Form: January 17, 2002

We have used scanning tunneling microscopy (STM), low-energy electron diffraction (LEED), and X-ray photoelectron spectroscopy (XPS) to investigate the thermal stability of Pd(111) islands and thin films on TiO_2(110)-(1 × 2). Two new nano-structures were observed to form on the surface of the Pd by annealing to 973 K. Atomic resolution STM images show a "pinwheel" super-structure. One domain has a $\begin{pmatrix}7 & 2\\5 & 7\end{pmatrix}$ unit cell with respect to the Pd(111) whereas the other domain has a $\begin{pmatrix}7 & 5\\2 & 7\end{pmatrix}$ unit cell. Coexisting with this phase is a structure consisting of zigzag rows that run along the close-packed directions of the Pd(111) islands. This has a rectangular unit cell incommensurate with both the substrate TiO_2(110) and the Pd(111) islands. STM shows these two structures merge with no noticeable domain barriers or steps, suggesting a close relationship between the two. LEED shows several distinct, overlapping patterns that can be identified with the surface structures observed; TiO_2(110)-(1 × 2), Pd(111)-(1 × 1), the hexagonal pinwheel structure, and the rectangular zigzag unit cell. XPS at normal and grazing emission show the encapsulating layer to be composed of TiO_x with Ti predominantly in $\sim 2^+$ or $\sim 3^+$ oxidation states. The proposed models are structurally consistent with the LEED and STM data and have stoichiometries of TiO and $TiO_{1.4}$, chemically consistent with the XPS spectra. The STM images of the zigzags bear a strong similarity to structures seen for annealed Pt islands on TiO_2(110)-(1 × 1) and TiO_x supported on Pt(111), while the pinwheel structure is similar to annealed Cr on Pt(111). We discuss the similarities of our structures to those seen before for these related systems.

I. Introduction

The strong metal−support interaction (SMSI) of oxide-supported metal catalysts was discovered by Tauster et al. in 1978.[1] This discovery, in part, has motivated much research into metal/oxide systems with an increasing number of surface science studies on single-crystal oxide-supported model catalysts.[2−25] Of particular relevance are various Pt/TiO_2 studies. Madey et al.'s X-ray photoelectron spectroscopy (XPS) and low-energy ion scattering spectroscopy (LEIS) experiments show that Pt supported on TiO_2(110) is encapsulated by titanium oxides TiO_x ($0 < x < 2$) after annealing in ultrahigh vacuum (UHV)[2,3] whereas Boffa et al.[26] used XPS, low-energy electron diffraction (LEED), and scanning tunneling microscopy (STM) to study the "reverse model catalyst" of TiO_x supported on Pt(111) leading to atomically resolved images. Most recently, the Pt/TiO_2(110) system has been investigated with STM, again successfully obtaining atomic-scale structures of a TiO_x layer.[4] Dulub et al.[4] question the relevance of reverse model catalysts and the TiO_x/Pt(111) system specifically, although their own images bear similarities to those published by Boffa et al.[26] Interestingly, recent first-principles density functional theory (DFT) calculations of the TiO_x/Pt(111) system have revealed a preference for the initial Pt interface layer to consist of Ti with an O overlayer.[25]

The SMSI state usually arises when metal/reducible metal oxide systems are heated under reducing conditions. However, Bowker and co-workers[5,6] have recently demonstrated novel SMSI phenomena on the Pd/TiO_2(110) model catalyst system which occurs by heating in an oxidizing environment of low pressure O_2. Here, O_2 preferentially adsorbs onto Pd nanoparticles then migrates (spills over) onto the surrounding titania accelerating the reoxidation of TiO_2(110).[27−29] This spillover/reoxidation process leads to burial of the Pd particles forming a new type of SMSI.[5,6] The more traditional SMSI state of Pd on TiO_2(110)-(1 × 1) formed by annealing in UHV has also been studied recently using coaxial impact-collision ion scattering spectroscopy (CAICISS) and reflection high-energy electron diffraction (RHEED) with the authors suggesting that the Pd is encapsulated by TiO_x ($x \approx 2$).[7]

Here, we show the formation of two coexisting SMSI states by heating Pd supported on the non cross-linked (1 × 2) reconstruction of TiO_2,[27,28] in UHV conditions. The resulting surface was analyzed using STM, LEED, and XPS. Our atomically resolved STM images show two types of surface structure. One has a complicated "pinwheel" structure reminiscent of Zhang et al.'s Cr/Pt(111) superstructure,[30,31] the other consists of rows of zigzags somewhat similar to images seen by Boffa et al.[26] and Dulub et al.[4] LEED gives two diffraction patterns that can be assigned to the two types of nano-structure, and XPS shows that the two new surface structures arise from encapsulation of the Pd with layers of composition TiO_x ($x \approx 1.4$ and $x \approx 1$). Section II describes the experimental procedure, Section III presents the results in three sub-divisions: *A. STM*,

* Author to whom correspondence should be addressed.
[†] Department of Chemistry, The University of Reading.
[‡] Department of Physics, The University of Reading.
[§] Boreskov Institute of Catalysis.

10.1021/jp0138328 CCC: $22.00
Published on Web 04/11/2002

B. LEED, and *C. XPS*. This is followed by a discussion of the results in Section IV, and finally, the summary and conclusions in Section V.

II. Experimental Section

The STM experiments were performed in a WA Technology variable temperature STM operated at room temperature with a base pressure of $\leq 1 \times 10^{-10}$ mbar. Empty states tunneling was used throughout with typical imaging parameters of 1.5 V and 0.1 nA.

The XPS measurements were taken in a separate chamber with a VSW photoelectron spectrometer using Mg Kα excitation and constant pass energy of 44 eV [Ag3d$_{5/2}$ full width at half-maximum (fwhm) = 1.2 eV] operated under a base pressure of $\leq 2 \times 10^{-10}$ mbar. The spectra were referenced to Cu 2p$_{3/2}$ (932.66 eV), Cu L_3MM (334.94 eV), Ag 3d$_{5/2}$ (368.27 eV), and Cu 3p$_{3/2}$ (75.13 eV) lines.

TiO_2 crystals (Pi-Kem) were supplied cut and polished to within 0.5° of the (110) plane. The surface, which was mainly the non cross-lined (1 × 2) reconstruction, but with some regions of (1 × 1) reconstruction, was prepared by sputter and anneal cycles up to 1200 K. Pd was deposited from high-purity Pd wire wrapped around a W filament onto the TiO_2(110) surface held at room temperature. Both chambers were equipped with LEED and the photographs in this article were obtained from the STM chamber using 3-grid VG optics. Deposition procedures were similar in both chambers, with Pd deposited until the TiO_2 substrate LEED patterns were extinguished and replaced by very faint Pd(111) patterns on a high background. The surfaces were postannealed at various temperatures for 20−25 min and the evolution of surface structure was followed by LEED. Structure formation was reproducible between experiments in different chambers and occurred in the same temperature range. Coverages were obtained using STM images in which the bare substrate areas define the surface plane upon which the Pd overlayer thickness was estimated. We assume that none of the Pd had dissolved into the TiO_2 substrate, and define a Pd monolayer (ML) as the two-dimensional Pd(111) packing density of 1.52×10^{15} atoms cm^{-2}.

III. Results

A. STM. Figure 1 shows a wide area STM scan (6000 Å × 6000 Å) of the Pd/TiO_2(110) surface. A thin film has formed on the surface. This follows deposition of Pd then annealing at ∼573 K for 25 min, ∼773 K for 20 min, and ∼973 K for 20 min. Figure 2 shows a higher magnification image (2000 Å × 2000 Å) of the same surface. Step edges on the film are now visible. The minimum step height observed of ∼2 Å [compared with 2.24 Å for the native Pd(111) surface] together with the pseudohexagonal holes suggest that a film of Pd(111) is grown on the surface. The depth of the holes range from ∼30−70 Å. Examination of these holes (inset) now reveals cross-linked (1 × 2) structure from the underlying substrate.[27,28,32] The presence of the exposed substrate in these holes implies the Volmer−Weber (VW) growth mechanism (3D islanding). The topmost layers of the Pd(111) surface generally appear elongated as indicated by the line, ***a***, in the figure. The volume of the Pd above this substrate layer allows an estimation of the Pd coverage of 20 ML.

The 1630 Å × 1630 Å (inset 13770 Å × 13770 Å) STM image in Figure 3 shows the surface formed from a slightly lower coverage of Pd (14 ML). Instead of a film, large, pseudohexagonal, flat-topped islands are formed similar to those seen by Dulub et al.[4] for Pt on TiO_2(110)-(1 × 1). The height

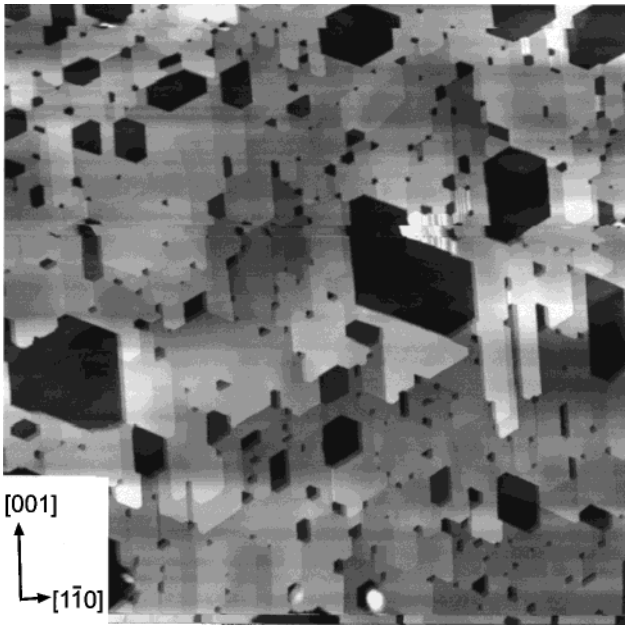

Figure 1. A 6000 Å × 6000 Å STM image of Pd/TiO_2(110)-(1 × 2) following annealing at 573 K for 25 min, 773 K for 20 min, and 973 K for 20 min.

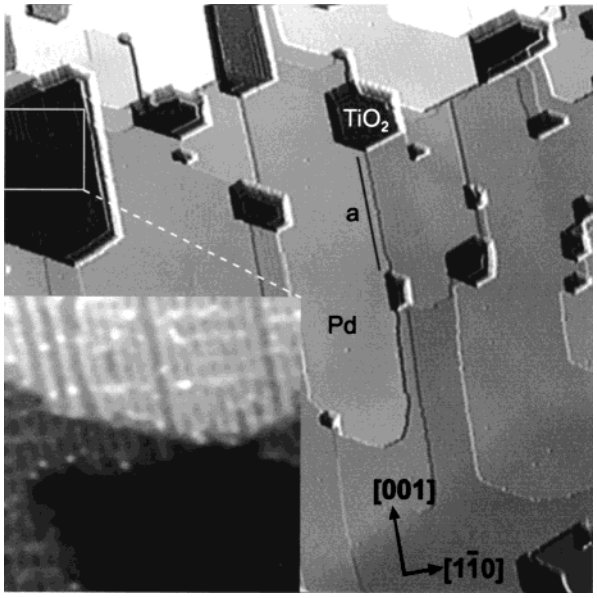

Figure 2. A 2000 Å × 2000 Å STM image of Pd/TiO_2(110)-(1 × 2) following annealing at 573 K for 25 min, 773 K for 20 min, and 973 K for 20 min. The inset is an enlarged area that shows cross-linked (1 × 2) rows. The azimuths are with respect to the substrate TiO_2(110) throughout this article. The line **a** indicates a step edge of the Pd surface layer which is extended in the [001] direction.

of these 3D islands are ∼80 Å. Widths range from ∼100 Å to ∼2000 Å. Again the substrate (1 × 2) rows can be seen, in line with VW growth. The same structures are apparent at high resolution on the surfaces of both the film and the islands. These structures are the pinwheel (outside) and the zigzag (center) structures shown in Figure 4. This image (360 Å × 360 Å) shows the two structures merging together with no step edges nor any noticeable domain barrier, suggesting a very close relationship between the two structures.

We will first focus on the pinwheel structure. A higher magnification image (105 Å × 105 Å) is shown in Figure 5a. The lattice spacing in all three directions are equivalent (∼3.25 Å) reflecting a true hexagonal structure. One of the pinwheels

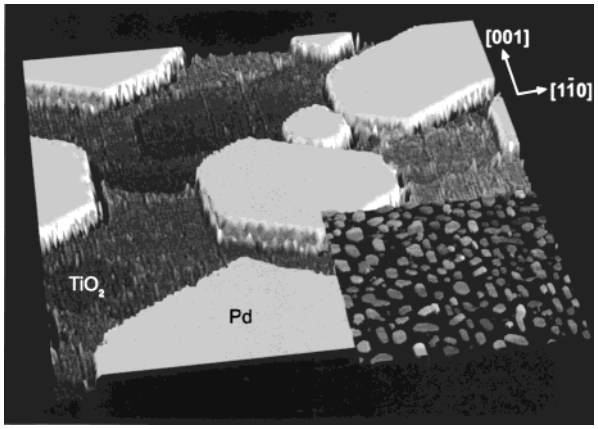

Figure 3. 3D representation of a 1630 Å × 1630 Å STM image of $Pd/TiO_2(110)$-(1 × 2) following annealing at 573 K for 25 min, 773 K for 20 min, and 973 K for 20 min. The inset is a 13770 Å × 13770 Å STM image of the same surface.

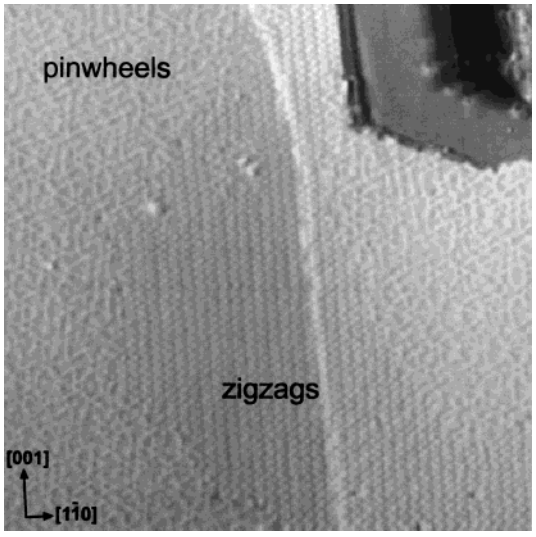

Figure 4. A 360 Å × 360 Å STM image showing zigzag areas (center) and pinwheel areas (outside).

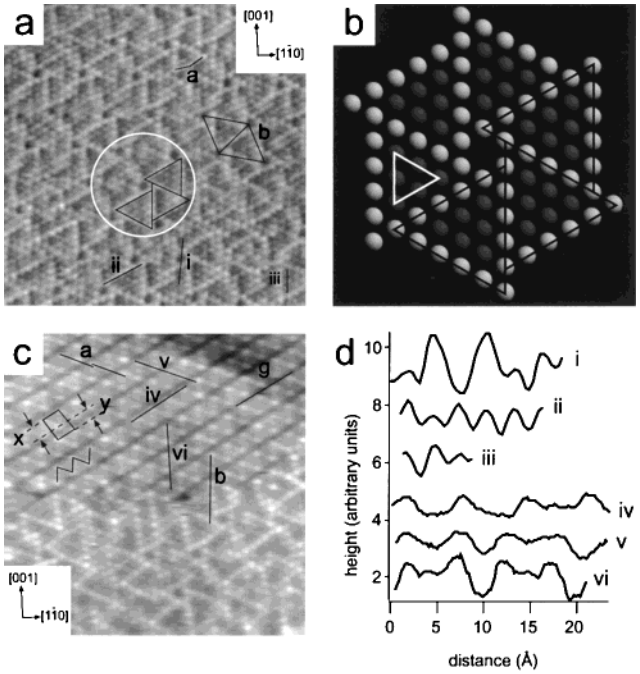

Figure 5. (a) A 105 Å × 105 Å STM image of the pinwheel structure. The circle highlights a pinwheel and the three triangles mark out part of the ideal pinwheel structure. The line, ***a***, indicates a bend in a spoke, and ***b*** indicates the superstructure. The lines, ***i***, ***ii***, and ***iii*** indicate line profiles shown in Figure 5d. (b) Schematic picture of the ideal pinwheel structure. Three 9 × 9 triangles are marked with black triangles as in (a), and an internal 3 × 3 triangle is marked with a white triangle. (c) A 101 Å × 101 Å STM image of an area showing the pinwheel structure (bottom) and the zigzag structure (top). The unit cell marked that of the zigzag structure. The central spot in the unit cell is off-center as indicated by the ratio ***x*:*y*** = 27:23. ***a*** marks two lines drawn along the zigzag diagonals; these indicate the phase shift as one goes across the troughs. ***g*** marks a glide-plane. ***b*** marks the rotation as one goes from the spokes of the pinwheel to the diagonal of the zigzag. The lines, ***iv***, ***v***, and ***vi*** indicate line profiles shown in Figure 5d. (d) Line profiles along the lines marked in Figure 5a and b. Profiles shown are taken from a processed image for clarity and therefore height information is not maintained, although measurements given in the text are taken from the raw data. The maximum peak-to-peak heights for each line profile are (i) = 1.2 Å, (ii) = 0.3 Å, (iii) = 0.3 Å, (iv) = 0.8 Å, (v) = 1.0 Å, and (vi) = 1.2 Å.

is circled. It is difficult to clearly define a unit cell due to the large size and imperfect ordering of the superstructure but we may describe an ideal pinwheel with six 6 × 6 triangles that interlock around a central hub, as shown in Figure 5b. Three near ideal triangles of this structure are drawn in this circled area in Figure 5a. The perimeter of each triangle has spots with large apparent height that form the "spokes" of the pinwheel. Many of these spokes are bent as indicated by the line, ***a***, in the figure. Enclosed within the spokes are 3 × 3 triangles containing 6 atoms that are imaged with lower apparent height. This gives the appearance of a central hexagon of raised spots that are simply part of the spokes. The line profile across a hub is shown in Figure 5d(i), as is the corrugation along a spoke and an internal triangle in Figure 5d(ii and iii). The corrugation across the hub, along the spokes, and along the internal triangles are ∼1.2 Å, ∼0.3 Å, and 0.3 Å ,respectively. Each pinwheel domain is chiral, in itself, but as both left-handed and right-handed domains are observed, we do not expect any chirality on the surface as a whole.

The 101 Å × 101 Å STM image in Figure 5c shows a zigzag area and a pinwheel area with high resolution. Looking first at the zigzag areas, straight dark troughs run in the close packed directions of the Pd as deduced from LEED, and the alignment of the Pd island edges as evidenced by STM, which are assumed to run in the close packed directions. The troughs are ∼4 Å wide with depths of ∼1 Å and a periodicity of 8.7 Å in the direction perpendicular to the trough direction. Between the troughs are the zigzags themselves which run parallel to the troughs. The zigzags consist of 3 spots in the diagonals, as indicated by the overlying zigzag in Figure 5c, and one faint spot between each of the zigzags. The spots at the apexes of the zigzags have a greater apparent height than those lying in the center of the zigzags which, in turn, lie apparently higher than the faint spots between the zigzags. The atomic spacing in the longitudinal direction of the zigzag rows is ∼3.25 Å, highlighted in Figure 5d(iv), although the intermediate spots are barely seen in the profile. Along the zigzag diagonals, the spacing is shorter − ∼2.9 Å, highlighted in Figure 5d(v and vi). The difference in these lattice spacings means that the structure is only pseudohexagonal. The rectangular unit cell of the zigzags, an example of which is indicated in the figure, has the dimensions 8.7 Å × 6.5 Å. Close inspection of this unit cell shows that the central spot is slightly offset from the center. The ratio **(*x*:*y*)** in the figure is 27:23. This is consistent with the guide-lines (marked ***a*** in the figure) drawn across the zigzag diagonals being offset as the troughs are traversed. A glide plane

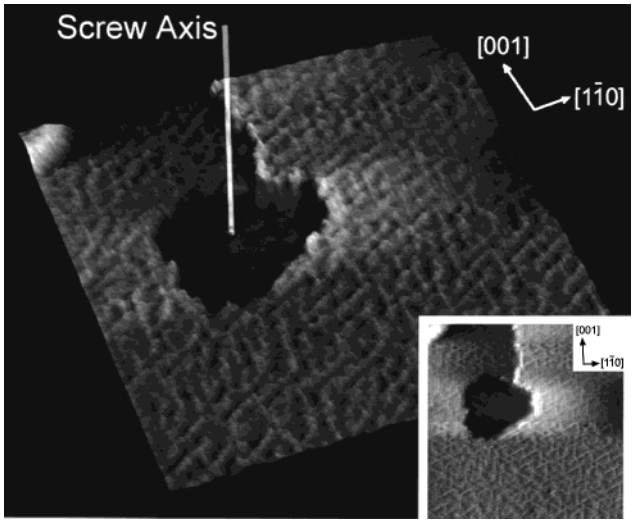

Figure 6. 3D representation 182 Å × 182 Å STM image of the pinwheel structure containing a screw dislocation. The dislocation is evidenced from the material surrounding the central depression in the image, which shows an apparently continuous structure, mismatched at the top of the image by one vertical step height. In this region the film is angled with respect to the underlying planar surface and although the origin of the dislocation is not clear, the structure is continuous around the dislocation.

is drawn (***g***) over one of the troughs. The glide plane is also evident in LEED (discussed below) and indicates a p2 mg space group for this structure. We would intuitively expect 3 zigzag domains rotated at 60° from each other based on the 3-fold symmetry of the underlying Pd(111). However, the zigzags run primarily in the [001] direction of the titania substrate with only a small number of domains seen rotated at ±60° to this majority phase.

Figure 5c also shows that the "spokes" of the pinwheel lead directly into the zigzags of the zigzag structure emphasizing the close relationship between the two. Interestingly, there is a 3−7° rotation going from the spoke to the zigzag as indicated ***b*** in the figure. It is difficult to give an exact angle due to an inherent bend in the spoke of the pinwheels. Figure 6 shows a 182 Å × 182 Å image of the pinwheel structure covering the Pd, which contains a screw dislocation centered on a void in the film. The axis of the screw dislocation is indicated with the resulting step edge running to the top of the image. The image shows that the pinwheel structure surrounds the defect. There is a large incidence of such screw dislocations in the film and these possibly play a role in dictating the handedness of the neighboring pinwheel domains.

B. LEED. The as-deposited Pd/TiO_2(110) surface displayed a faint hexagonal pattern arising from facets of Pd(111) (not shown here). Figure 7 shows a LEED pattern of this surface after further annealing to 773 K for 20 min. The same hexagonal pattern can be seen as previously but with a reduced background and sharper spots. Annealing at 973 K for another 20 min gives a complicated LEED structure, shown in Figure 8a, which has essentially 4 patterns superimposed and is de-convoluted as follows; the solid rectangle labeled ***a*** is the pattern generated by exposed regions of the TiO_2(110)-(1 × 2) substrate; the solid hexagon labeled ***b*** corresponds to Pd(111) integral order spots that has a real space nearest neighbor distance of 2.75 Å; the dash−dotted rectangle labeled ***c*** derives from the zigzag unit cell basis (spots were observed to be missing due to the glide plane in other LEED images not shown here); finally, the pair

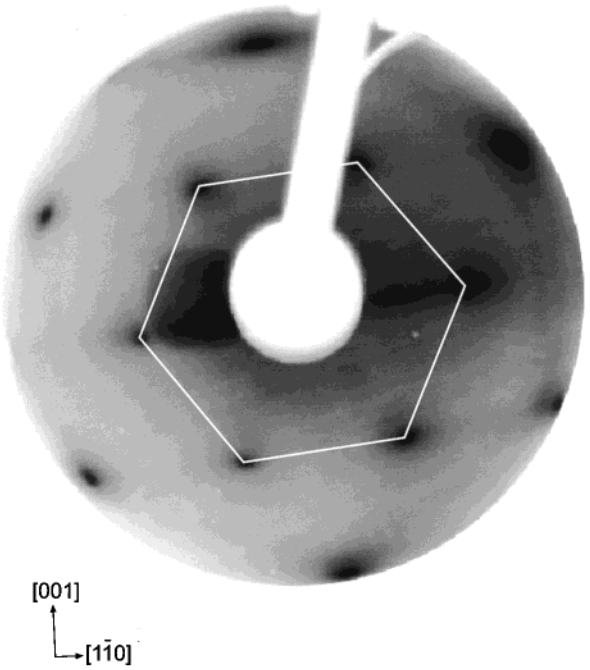

Figure 7. LEED pattern of the Pd/TiO_2(110)-(1 × 2) surface following annealing to 573 K for 25 min, then 773 K for 20 min. The hexagonal pattern seen corresponds to Pd(111).

of dashed hexagons labeled ***d*** belong to the basis of the pinwheel structure and are rotated ±3° with respect to the Pd(111) substrate.

From the dimensions of the known TiO_2 and Pd lattice constants we can deduce from LEED the size of the unit cells and basis vectors of the two overlayers. We find a real-space nearest neighbor distance of ∼3.3 Å and a hexagonal lattice for the pinwheel basis vectors. The zigzag rectangular cell has real-space dimensions of ∼8.7 Å × ∼6.5 Å. Notice that in the [1$\bar{1}$0] direction, this rectangle is commensurate with the TiO_2 substrate unit length in a 2:3 ratio. The LEED patterns from all these structures are shown schematically and to scale in Figure 8b for clarity.

Figure 9 shows fast Fourier transforms (FFT) of STM images from (a) the pinwheel structure and (b) the zigzag structure. The pinwheel gives a complicated hexagonal pattern with floreting due to the superstructure but not particularly reminiscent of any LEED component seen, aside from the hexagonal symmetry. The large hexagon, marked ***h***, corresponds to the lattice spacing of the surface layer.

The FFT of the zigzag area has a rectangular unit cell with dimensions consistent with the LEED pattern and that assigned to the STM image.

C. XPS. The same preparation used to produce the Pd film was used here. XPS data were taken directly following Pd deposition and after annealing to ∼970 K. After annealing, an identical LEED pattern to that shown in Figure 8a was obtained giving evidence that a Pd/TiO_2(110)-(1 × 2) surface comparable to those seen with STM was prepared. Figure 10a shows the Ti 2p region at normal emission angle directly after Pd deposition and after annealing. The as-deposited surface shows no shift nor any change in shape in these Ti^{4+} 2p doublets (marked A) when compared with our spectra of the clean TiO_2(110) (not shown) and various XPS spectra from the literature. [13,33] After annealing, the 2p peaks from Ti^{4+} are still present, but a new doublet feature, indicated B in Figure 10a, appears at a lower binding energy to the Ti^{4+} peak. The splitting of the doublet B is the same as that of doublet A and is attributable to 2p peaks

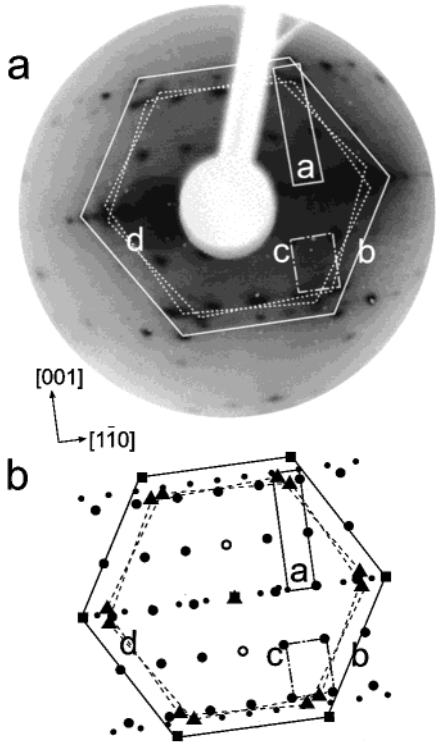

Figure 8. (a) LEED pattern of the Pd/TiO_2(110)-(1 × 2) surface following annealing to 573 K for 25 min, 773 K for 20 min, then 973 K for 20 min. Four patterns are observable here. The solid rectangle ***a*** represents the TiO_2(110)-(1 × 2) substrate, the solid hexagon ***b*** represents the Pd(111) film, the dashed−dotted rectangle ***c*** represents the zigzag unit cell. The two dotted hexagons ***d*** rotated ±3° to the Pd(111) hexagon represent the lattice of the pinwheel structure. (b) A schematic representation of the LEED pattern shown in Figure 8(a). ***a***, ***b***, ***c***, and ***d*** represent the same unit cells as in (a). Small circles represent the TiO_2(110)-(1 × 2) spots, squares show the Pd(111) spots, large filled circles denote the zigzag spots, large open circles show the missing spots due to the glide-plane, and triangles designate the pinwheel spots.

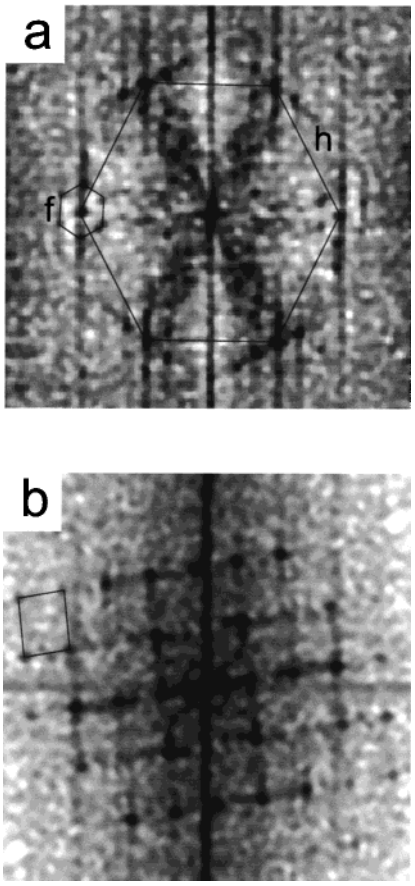

Figure 9. (a) FFT of a pinwheel STM image. A floreted hexagonal pattern is obtained. The hexagon and the florets are marked ***h*** and ***f***, respectively. (b) FFT of a zigzag STM image. Rectangular symmetry is obtained and a unit cell is marked. (a) and (b) are not shown on the same length scale.

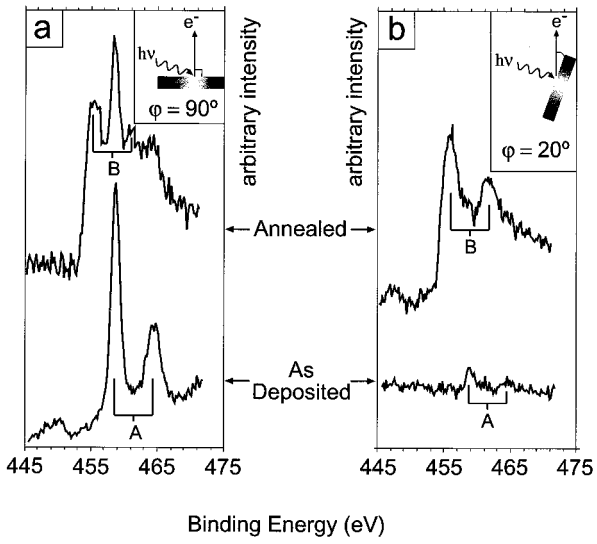

Figure 10. XPS spectra of Pd/TiO_2(110)-(1 × 2) as-deposited and following annealing to 973 K for 20 min. The postanneal spectra are drawn above the as-deposited spectra. In the as-deposited data, 2p doublets corresponding to Ti^{4+} are seen and marked A in the figure. After annealing a new Ti 2p doublet, marked B, is seen with a lower binding energy than Ti^{4+}. (a) Normal emission data. (b) Data taken at grazing emission angle, $\varphi = 20°$, from the surface.

of Ti^{n+} in a reduced state ($n = 2$ or 3). The reduced Ti 2p peaks (doublet B) are at 2.8 eV lower binding energy than the original Ti^{4+} 2p peaks (doublet A). To achieve increased surface sensitivity, the equivalent spectra, shown in Figure 10b, were obtained at a grazing emission angle, $\psi = 20°$ from the surface as shown in the figure. The as-deposited surface shows a much reduced Ti^{4+} signal due to high coverage of the film, the 2p peak is, however, unchanged in position from that of the clean TiO_2(110).[13,33] Following annealing the spectrum is dominated by the doublet B due to reduced species, as seen in the normal emission. However, the intensity in the Ti^{4+} region (appearing as a shoulder between the peaks of doublet B) is approximately the same as in the as-deposited spectrum.

IV. Discussion

We first discuss the chemical composition of the surface layer before examining structural models of the overlayer. The presence of Ti^{4+} 2p peaks in the normal and grazing emission spectrum for the as-deposited Pd/TiO_2(110)-(1 × 2) surface shown in Figure 10a,b indicates the presence of some bare titania. The significant drop in intensity with moving to grazing emission shows that this signal derives from the substrate, probably from small holes or thin layers in the film. After annealing the surface the Ti^{4+} intensity is similar to the as-deposited film in both the grazing and normal emission spectra, which suggests little change in the total area of the exposed TiO_2(110)-(1 × 2). The appearance of TiO_2 LEED spots at this stage is due to ripening of these holes to produce fewer but larger holes which allow the TiO_2 to produce a diffraction pattern due to the larger exposed domains. This is consistent

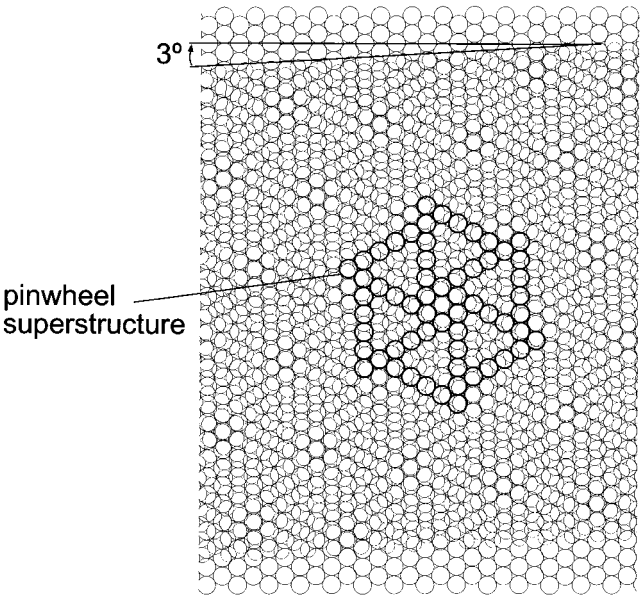

Figure 11. A hexagonal lattice of 3.25 Å periodicity is rotated 3° upon a lattice of 2.75 Å periodicity giving rise to the superstructure drawn in bold. This pattern is identical to the ideal pinwheel shown in Figure 5b.

with both the STM images presented here in Figures 2 and 3 and other work[10,11] that also indicate VW growth.

Annealing introduces new features in the XPS spectrum at 2.8 eV lower binding energy than the Ti^{4+} peaks, revealing the presence of reduced Ti states. There is no concomitant change in Pd oxidation state (spectra not shown), so Ti must be present in the form of TiO_x ($1 \leq x \leq 2$). Comparing the shape of the Ti 2p peak with those published by Guo et al.[34] for a Ti_2O_3-(0001) film grown on Mo(110), we see a peak similar to theirs convoluted with a Ti state at even lower binding energy, therefore indicating the presence of both $\sim Ti^{2+}$ and $\sim Ti^{3+}$ states. The intensity of these reduced states is not significantly reduced on moving from normal to grazing emission, whereas the Ti^{4+} signal from the exposed TiO_2 substrate is severely attenuated. This clearly indicates the reduced states originate from a topmost layer on the Pd film and not from the exposed TiO_2 substrate.

These XPS data closely resemble those taken for Pt/TiO_2-(110) following annealing to 800 K [2] which is interesting considering the similarity of the zigzags seen in STM reported here and those observed by Dulub et al.[4] for $Pt/TiO_2(110)$-(1×1). A quantitative analysis of these and related XPS spectra will be published in a separate article.[35]

Having established that the layer which encapsulates the Pd contains $\sim$TiO and $\sim Ti_2O_3$, we now consider the geometry of the layers. The LEED data show that we have one lattice with hexagonal symmetry and 3.25 Å periodicity rotated at $\pm 3°$ with respect to the Pd lattice which itself has a periodicity of 2.75 Å. A hexagonal lattice with 3.25 Å periodicity rotated at 3° to an underlying 2.75 Å lattice as dictated by the LEED pattern is drawn in Figure 11. Atoms in the top layer which lie on bridge sites or near atop sites will be both geometrically raised and under-coordinated in comparison to the atoms which sit lower in 3-fold hollow sites. So, in STM the atoms which sit in 2-fold and nearly atop sites will appear bright compared with those in 3-fold hollow sites. Thus this purely geometrical model is consistent with the STM results, the brighter spokes corresponding to atoms in 2-fold and near atop sites and the darker internal triangles corresponding to atoms in the 3-fold hollows.

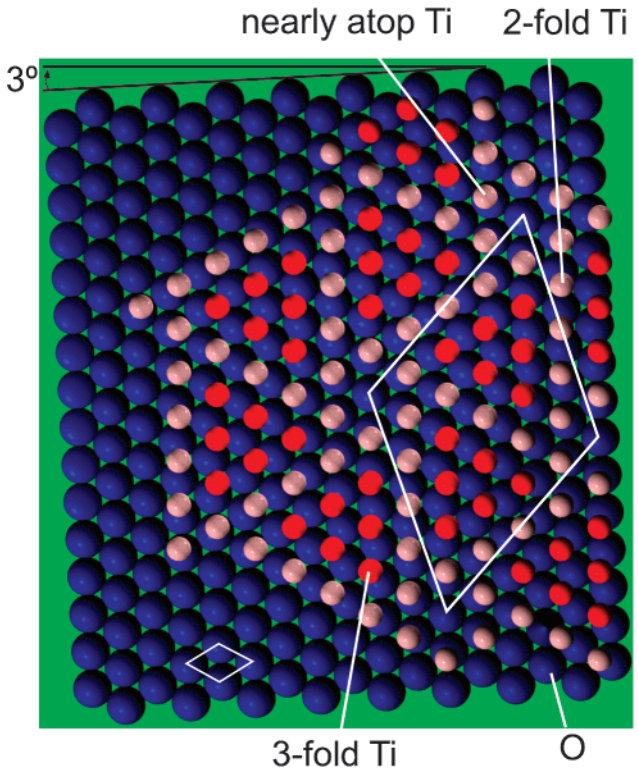

Figure 12. Our model for the pinwheel. A layer of O is placed on the Pd 3-fold hollow sites (either all fcc or all hcp sites) with exactly the same lattice spacing. On top of the O layer, a Ti layer is added with a lattice spacing of 3.25 Å and rotated at 3° to the Pd and therefore the O lattice. The small unit cell of the Pd(111) is indicated as is the large unit cell of the superstructure. Large blue spheres are O atoms, small red spheres are Ti atoms in 3-fold hollow sites, and small pink spheres are Ti atoms in 2-fold (bridge) sites or nearly atop sites. The Pd substrate is depicted as the green block.

The figure shows an arrangement of spokes drawn in bold that make a pinwheel.

The arrangement of atoms in the internal triangles of this geometric model is reminiscent of the TiO(111) surface which has a lattice spacing of 3.0 Å, so we propose the following model for the pinwheel structure. An O layer with hexagonal symmetry and a lattice spacing equal to the Pd(111) lattice of 2.75 Å is placed on the Pd(111) surface commensurately with the O in 3-fold hollow sites (all fcc or all hcp). Next, Ti is placed on top of this layer with a lattice spacing of 3.25 Å but rotated at 3° with respect to the O layer and therefore the Pd-(111) layer as shown in Figure 12. The sites in the center of the pinwheels correspond to exactly atop positions that we suggest are highly unfavorable and thus not populated by Ti. The superstructure has a $\begin{pmatrix} 7 & 2 \\ 5 & 7 \end{pmatrix}$ unit cell with respect to the Pd-(111) in the domain shown, whereas the other reflection domain (not shown) has a $\begin{pmatrix} 7 & 5 \\ 2 & 7 \end{pmatrix}$ unit cell. The unit cell vectors are both 17.2 Å. The model has a stoichiometry of $TiO_{1.4}$ consistent with XPS data. In TiO and TiO_2, states just above the Fermi level are dominated by Ti 3d, so we expect tunneling to be into Ti atoms, and therefore our model has Ti exposed to vacuum rather than O. Each spot in the STM presumably corresponds to a Ti atom.[36,37] This model is somewhat similar to a recently proposed model of VO_2 supported on Pd(111) by Surnev et al.[38] where an O layer was also placed commensurately on Pd(111).

The bend in the spokes seen in Figure 5 can easily be explained with our model. It simply arises from Ti atoms in

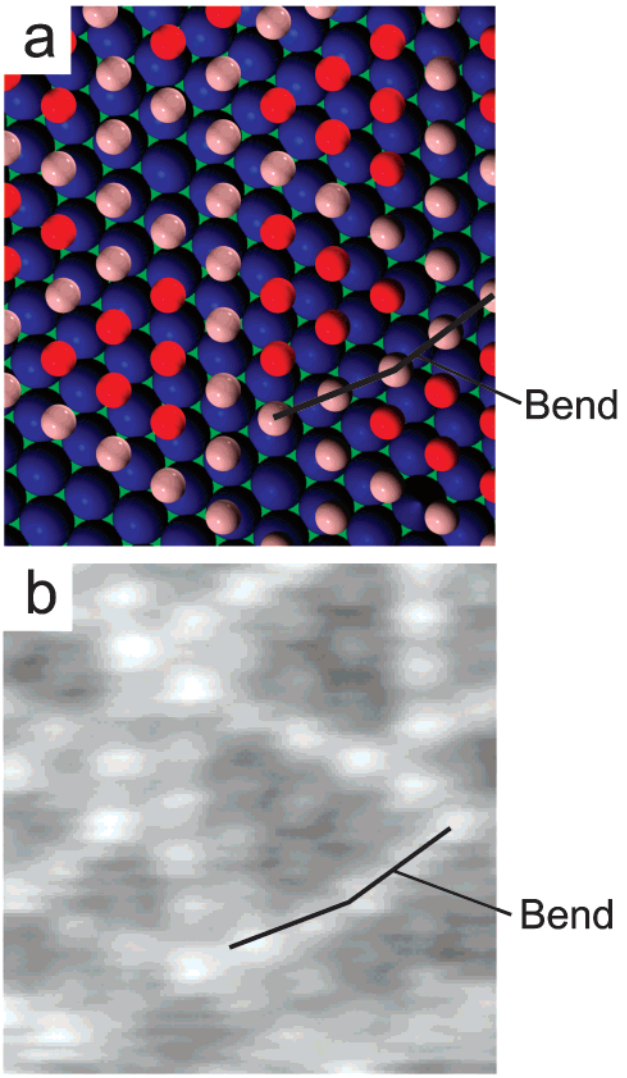

Figure 13. (a) As Figure 12, but zoomed in, and showing a bend in the spokes due to some Ti atoms in the spokes relaxing toward 3-fold sites. (b) An STM image expanded and rotated to approximate the dimensions of the model. The bend is marked.

the spokes moving toward the more favored 3-fold hollows sites as shown in Figure 13.

The FFT pattern in Figure 9a does not match the LEED pattern further than the hexagonal symmetry for two reasons. First, STM essentially records information from the very top layer of the surface, and the 3° rotation is with respect to the underlying layers. Hence, only the rotated overlayer can be seen in the FFT, with no information retained regarding its orientation with respect to the underlying film. Second, florets are not seen in LEED because the FFT was taken from a particularly well-ordered area where a hexagonal superstructure can be seen as shown in Figure 5a. However, there are many less well-ordered pinwheel areas that will contribute to the LEED pattern so that whilst the 3.25 Å lattice is observed no superstructure can be seen.

In the investigations of Zhang et al.[30,31] Cr was deposited onto Pt(111) and annealed, with the resultant surface forming a surface Cr−Pt alloy. A superstructure described as a "wagon wheel" was observed with a simplified model[30] that is almost identical to our ideal structure shown in Figure 5b except that their spokes have 7 atoms along them, and therefore the internal triangles are 4 × 4. We prefer to term the structure described here as a pinwheel because a wagon wheel might imply a centrosymmetric structure that is not consistent with the STM. It is likely that similar geometric arguments underpin the formation of the wagon wheels of Zhang et al.[30,31] and perhaps revealing that the 17.3 Å unit cell vector observed for the wagon wheels is almost identical to our pinwheel unit cell dimension of 17.2 Å. This discrepancy simply arises from the difference lattice constants of Pd and Pt. It is possible that our pinwheel structure derives from some analogous Pd−Ti surface alloy that is oxidized during our preparation but it is difficult to establish this experimentally. Ab initio calculations may be able to offer some insight, at least into the relative stability of such an alloyed system. Later in this section a comment is made on some recent ab initio calculations by Jennison et al.,[25] based on oxide systems, which may assist in further understanding this structure. The screw dislocation in Figure 6 shows that the structure is stable enough to remain intact over large defect structures.

We now turn to the zigzag structure, which shows only a single domain in LEED. It is interesting that the zigzags run primarily in the [001] direction of the substrate. This suggests that most domains are pinned in the [001] direction by the substrate TiO_2(110). However, as the TiO_2 layer is up to 80 Å below the surface, any pinning must be indirect. There may be some anisotropy in the Pd(111) layer between the TiO_2 and the surface layer which pins the zigzag rows in this direction. Returning to Figure 2, it can be seen that the surface layers are extended in the [001] direction as also observed by Evans et al.[14] This is due to more facile diffusion of Pd along the [001] direction of TiO_2(110).[11] Now, if Pd(111) islands are elongated in the [001] direction then it follows that zigzag domains aligned in this direction will be significantly larger than domains which run at ±60° to this direction. Therefore the contribution to the LEED pattern is dominated by domains that run in this [001] direction.

The STM and the LEED data suggest a rectangular unit cell with dimensions 8.67 Å × 6.5 Å and the STM showed further that the lattice of the zigzags is only pseudohexagonal and is actually based on a centered rectangular unit. This is consistent with the FFT in Figure 9b where no hexagonal symmetry is obtained. The model in Figure 14 is constructed with this in mind. For clarity, we will define the longitudinal direction of the zigzags as [001] and the direction perpendicular to this as [1$\bar{1}$0]. For the majority of the domains, these directions will also correspond to the substrate TiO_2(110) directions. The model consists of rafts of a centered rectangular O lattice with a cell of 4.7 Å × 3.25 Å, marked β in the figure, separated by each other in the [1$\bar{1}$0] direction by ∼4 Å. Ti atoms then bridge across each O atom in the [001] direction. The α unit cell size is 8.67 Å × 6.5 Å consistent with LEED and STM. The central Ti atom in the α unit cell is offset to exactly the same amount as the central spot in the STM such that $\boldsymbol{x}$:$\boldsymbol{y}$ = 27:23. This makes the lattice spacings 3.25 Å in the [001] direction and 2.86 Å in the zigzag diagonals consistent with the STM measurements in Figure 5c and d. Guide-lines, marked ***a*** in the figure, are equivalent to those in Figure 5c showing a phase shift in the diagonals of the zigzag as one travels from one zigzag row to another. The smaller unit cell, marked β, of the O lattice is not seen in LEED because the rafts are not in phase in the [1$\bar{1}$0] direction.

The contrast across the zigzags could arise from relaxations which result in a buckling of the surface. We do not understand why the zigzag unit cell size in the [1$\bar{1}$0] direction is exactly 2/3 that of TiO_2(110)-(1 × 2) but surmise that it is probably just coincidental. The model has a stoichiometry of TiO consistent with the XPS data and furthermore, the different

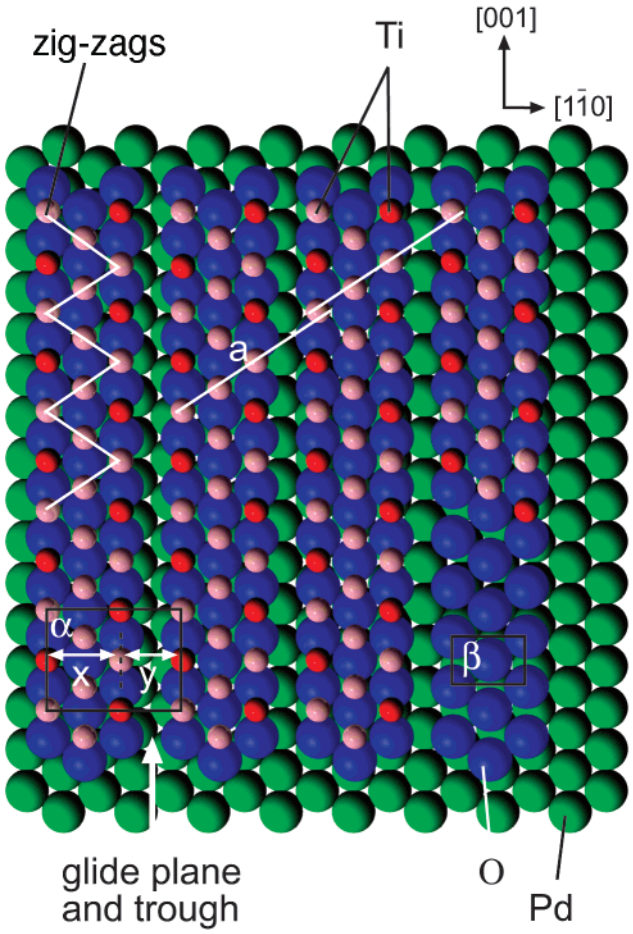

Figure 14. Our zigzag model. This consists of rafts of a centered rectangular O lattice which run in the [001] direction separated by troughs in the [001] direction. Ti atoms bridge O atoms in the [001] direction. Large, green spheres indicate Pd atoms, large blue spheres represent O atoms, small pink spheres represent Ti atoms in zigzags, and small red spheres represent Ti atoms in the internal triangles. The cell of the O lattice is marked β, but note that this does not translate in the [1$\bar{1}$0] direction. The unit cell α marks the unit cell of the zigzag structure. The central Ti atom in the unit cell is off-center as indicated by the ratio $x:y = 27:23$. ***a*** marks two lines drawn along the zigzag diagonals; these indicate the phase shift as one goes across the troughs. The troughs are also glide-planes as identified by LEED.

stoichiometries in the models proposed for this zigzag structure and the pinwheel structure supports the idea of mixed oxidation states leading to the convoluted peak in Figure 10.

Our STM images of the zigzag structure shares common themes with both the images seen by Dulub et al.[4] for a 25 ML deposit of Pt on TiO_2(110)-(1 × 1) annealed at 473 K for 30 min, 973 K for 5 min, and 773 K for 30 min, and the images Boffa et al.[26] obtained for a ∼1−1.5 ML thin film of TiO_2 deposited onto Pt(111). In the case of Dulub et al.[4] zigzags broader than ours ran in the [001] direction of the TiO_2(110) substrate separated in the [1$\bar{1}$0] direction by dark grooves which also run in the [001] direction. While Boffa et al.[26] do not observe zigzags, stripes narrower than ours with pseudohexagonal internal features were seen separated by dark grooves which run parallel to the stripes. It is likely that the three striped Pd/TiO_2, Pt/TiO_2, and TiO_2/Pt systems are related and that with some small modifications our model could explain these other images.

Ab initio calculations on the TiO_x/Pt(111) system by Jennison et al.[25] show a preferred Ti−Pt interface decorated by O. If the same were true for the TiO_x/Pd(111) interface then the layer sequence of Ti and O atoms would be reversed for our pinwheel and zigzag structures. In such a case the geometrical arguments presented above would still hold, with both structures looking identical in STM since the Ti states would be imaged through the O overlayer. However, the calculations by Jennison et al.[25] crucially rely on the atoms at the apexes of their extended zigzags being Ti at the surface for stability. With our shorter zigzags this would imply that all imaged surface atoms should be Ti. Therefore, the model for the zigzag structure shown in Figure 14, which consists of Ti atoms over a hexagonal raft of O atoms still appears the most plausible configuration. Moreover, since the pinwheel and zigzag structures have a common structure, as observed by the smooth interface in STM, the implication is that the pinwheel structure would also have a Ti−O surface layer, as shown in Figure 12. Furthermore, it is possible that the system is a surface Ti terminated multilayer (e.g., $(TiO)_n$−Ti−Pd) although substantial further work would be required to confirm this complex possibility.

That reverse model catalysts are comparable to SMSI states is further emphasized by the close relation between our work and very recent work concerning the growth of vanadium oxides on Pd(111).[38] Three types of VO_x layers were seen to coexist; a hexagonal V_2O_3 layer and two VO_2 layers, one with rectangular symmetry, the other with hexagonal symmetry. This work, compounded with ours, shows that reducible oxides grown on metal substrates may often show mixed oxidation states at the surface that can have serious implications for reactivity, in particular selective reactivity over different parts of the surface.

V. Summary and Conclusions

We have prepared two new SMSI states for Pd supported on TiO_2(110)-(1 × 2) which are very closely related. XPS corroborated the presence of two species at the surface with approximate stoichiometries ∼Ti_2O_3 and ∼ TiO. In both cases, a two atomic layer thick film of TiO_x encapsulates >40 Å thick Pd islands to form these new structures. For both models, the O layer is sandwiched between the Pd layer and the Ti layer that terminates the surface. The models proposed were consistent with the LEED symmetry and had compositions of $TiO_{1.4}$ for the pinwheel structure and TiO for the zigzag structure consistent with the XPS data.

The pinwheel structure shows the same geometry as the surface alloy observed by Zhang et al.[30,31] for Cr grown on Pt(111) whereas the zigzag structure was similar to both titania encapsulated Pt supported on TiO_2(110)-(1 × 1)[4] and a thin film of TiO_2 grown on Pt(111).[26] The latter is an example of a reverse model catalyst. Our work therefore suggests that reverse model catalysts *do* provide a good basis for investigation of SMSI effects.

Finally, it would be useful to perform ab initio calculations to test the stability of both our models, variations of them, and surface PdTi alloys with and without the Ti component oxidized. The computational effort could be minimized by ignoring the titania layer which is >40 Å below the surface anyway, and using a Pd(111) substrate.

Acknowledgment. R.B. and C.L.P thank Toyota Motor Corporation for the provision of PDRF positions, N.P. and R.D.S. are grateful to the EPSRC (UK) and Johnson Matthey PLC for the provision of CASE awards. P.M. thanks EPSRC ROPA (UK) for funding the PDRF position, and R.I.K thanks the Royal Society for funding the visit to Reading.

References and Notes

(1) Tauster, S. J.; Fung, S. C.; Garten, R. L. *J. Am. Chem. Soc.* **1978**, *100*, 170.

(2) Pesty, F.; Steinrück, H. P.; Madey, T. E. *Surf. Sci.* **1995**, *339*, 83.
(3) Steinrück, H. P.; Pesty, F.; Zhang, L.; Madey, T. E. *Phys. Rev. B* **1995**, *51*, 2427.
(4) Dulub, O.; Hebenstreit, W.; Diebold, U. *Phys. Rev. Lett.* **2000**, *84*, 3646.
(5) Bennett, R. A.; Stone, P.; Bowker, M. *Catal. Lett.* **1999**, *59*, 99.
(6) Bowker, M.; Smith, R. D.; Bennett, R. A. *Surf. Sci.* **2001**, *478*, L309.
(7) Suzuki, T.; Souda, R. *Surf. Sci.* **2000**, *448*, 33.
(8) Pang, C. L.; Raza, H.; Haycock, S. A.; Thornton, G. *Surf. Sci.* **2000**, *460*, L510.
(9) Højrup Hansen, K.; Worren, T.; Stempel, S.; Lægsgaard, E.; Bäumer, M.; Freund, H.-J.; Besenbacher, F.; Stensgaard, I. *Phys. Rev. Lett.* **1999**, *83*, 4142.
(10) Xu, C.; Lai, X.; Zajac, G. W.; Goodman, D. W. *Phys. Rev. B* **1997**, *56*, 13464.
(11) Jak, M. J. J.; Konstapel, C.; van Kreuningen, A.; Chrost, J.; Verhoeven, J.; Frenken, J. W. M. *Surf. Sci.* **2001**, *474*, 28.
(12) Møller, P. J.; Wu, M.-C. *Surf. Sci.* **1989**, *224*, 265.
(13) Schierbaum, K. D.; Fischer, S.; Torquemada, M. C.; de Segovia, J. L.; Román, E.; Martín-Gago, J. A. *Surf. Sci.* **1996**, *345*, 261.
(14) Evans, J.; Hayden, B. E.; Lu, G. *Surf. Sci.* **1996**, *360*, 61.
(15) Bird, D. P. C.; de Castilho, C. M. C.; Lambert, R. M. *Surf. Sci.* **2000**, *448*, L221.
(16) Chun, W. J.; Asakura, K.; Iwasawa, Y. *J. Phys. Chem. B* **1998**, *102*, 9006.
(17) Berkó, A.; Solymosi, F. *J. Phys. Chem. B* **2000**, *104*, 10215.
(18) Gan, S.; El-azab, A.; Liang, Y. *Surf. Sci.* **2001**, *479*, L369.
(19) Verdozzi, C.; Jennison, D. R.; Schultz, D.; Sears, M. P. *Phys. Rev. Lett.* **1999**, *82*, 779.
(20) Valden, M.; Lai, X.; Goodman, D. W. *Science* **1998**, *281*, 1647.
(21) Dixon, R. A.; Egdell, R. G. *Surf. Sci.* **2000**, *452*, 207.
(22) Campbell, C. T. *Surf. Sci. Rep.* **1997**, *27*, 1.
(23) Henry, C. R. *Surf. Sci. Rep*. **1998**, *31*, 235.
(24) Bäumer, M.; Freund, H.-J. *Prog. Surf. Sci.* **1999**, *61*, 127.
(25) Jennison, D. R.; Dulub, O.; Hebenstreit, W.; Diebold, U. *Surf. Sci. Lett.* **2001**, *492*, L677.
(26) Boffa, A. B.; Galloway, H. C.; Jacobs, P. W.; Benítez, J. J.; Batteas, J. D.; Salmeron, M.; Bell, A. T.; Somorjai, G. A. *Surf. Sci.* **1995**, *326*, 80.
(27) Bennett, R. A.; Stone, P.; Price, N. J.; Bowker, M. *Phys. Rev. Lett.* **1999**, *82*, 3831.
(28) Stone, P.; Bennett, R. A.; Bowker, M. *New J. Phys.* **1999**, *1*, 1.1; http://www.njp.org/.
(29) Bennett, R. A. *Phys. Chem. Commun.* **2000**, *3*.
(30) Zhang, L.; van Ek, J.; Diebold, U. *Phys. Rev. B* **1999**, *59*, 5837.
(31) Zhang, L.; van Ek, J.; Diebold, U. *Phys. Rev. B* **1998**, *57*, R4285.
(32) Murray, P. W.; Condon, N. G.; Thornton, G. *Phys. Rev. B* **1995**, *51*, 10989.
(33) Göpel, W.; Anderson, J. A.; Frankel, D.; Jaehnig, M.; Phillips, K.; Schäfer, J. A.; Rocker, G. *Surf. Sci.* **1984**, *139*, 333.
(34) Guo, Q.; Oh, W. S.; Goodman, D. W. *Surf. Sci.* **1999**, *437*, 49.
(35) Kvon, R. I.; Morrall, P.; Bowker, M. To be submitted.
(36) Ahuja, R.; Eriksson, O.; Wills, J. M.; Johansson, B. *Phys. Rev. B* **1996**, *53*, 3072.
(37) Diebold, U.; Anderson, J. F.; Ng, K.-O.; Vanderbilt, D. *Phys. Rev. Lett.* **1996**, *77*, 1322.
(38) Surnev, S.; Kresse, G.; Ramsey, M. G.; Netzer, F. P. *Phys. Rev. Lett.* **2001**, *87*, 086102.